A comparative study of transient characteristics of argon and argon-hydrogen pulse modulated induction thermal plasma

A Comparative Study of Transient Characteristics of Argon and Hydrogenated-Argon Pulse-Modulated Induction Thermal Plasma

M. M. Hossain, *Student Member, IEEE*, Y. Hashimoto, Y. Tanaka, K. C. Paul, *Member, IEEE*, and Tadahiro Sakuta, *Member, IEEE*

***Abstract*—Solving a time-dependent two-dimensional local thermodynamic equilibrium (LTE) model simulation of Ar and Ar–H_2 atmospheric pressure, a high-power RF-induction thermal plasma was performed. The effects of shimmer current level (SCL) in pulse-modulated mode and hydrogen concentrations on different flow fields were predicted. The radiation intensities of ArI (751 nm) for different SCL were calculated from the temperature fields. For the same operating conditions as simulation, plasma was successfully generated in pulse-modulated mode and spectroscopic measurements were carried out to investigate the effects of SCL upon temporal plasma properties. Response times (rising, falling, on-delay, and off-delay time) of temporal radiation intensity were crosschecked for both experimental and simulated ones. The rising time increased gradually with the decrease of SCL, though the falling time remained almost unchanged with SCL. For example, for Ar plasma at 86%, 79%, 72%, 65%, 50%, and 40% SCL the rising times were 2.7, 3.0, 3.4, 3.4, 3.6, and 3.8 ms, respectively. And for Ar–H_2 plasma (2.4% H_2), at 87%, 77%, 72%, 63%, 55%, and 45% SCL, rising times were 2.5, 3.0, 3.0, 3.4, 3.7, 3.9, and 4.0 ms, respectively. Hydrogen inclusion slowed down the plasma response during the off-to-on pulsing transition at lower SCL and constricted the plasma axially. Finally, part of the simulated results was compared with experimental determinations and acceptable agreements were found. The discrepancies, in few cases, explicated mainly that the LTE assumption did not prevail in pulse-modulated plasma, especially around the on-pulse transition.**

***Index Terms*—Duty factor, integrated radiation intensity and response time, local thermodynamic equilibrium (LTE), non-LTE, pulse-modulated induction plasma, shimmer current level (SCL).**

I. Introduction

As a source of high enthalpy and high density of chemical species, induction thermal plasma has become an important tool in new materials processing and destruction of toxic waste materials. Although some applications of radio frequency induction plasma technology, such as plasma vapor deposition, plasma cutting, atmospheric and vacuum plasma spraying, are already well established, current research activities are mainly for the optimization and refinement of these processes; intelligent processing and automation are still in the forefront of research endeavors.

Pulse modulation technique for induction thermal plasma (ITP) discharge is a new approach where solid-state devices are used in generating high-amplitude and high-frequency coil current. The use of solid-state devices not only improves the matching efficiency, but also offers the easy control of plasma energy. Control of plasma energy by changing duty factor (DF) or shimmer current level (SCL), keeping the maximum power level unchanged, is an attractive method for controlled plasma operation. Pulse-modulated plasma may have potential industrial applications in plasma nitriding, pulsed laser deposition, pulsed plasma surface treatment, pulsed ion beam treatment, pulsed CVD, and pulsed magnetron sputtering. A number of authors have proposed theoretical models for the LTE [1]–[3] and non-LTE [4]–[6] conditions of RF-induction plasmas in a steady-state approach. A few works have been reported elucidating the transient characteristics of RF-ITP [7]–[12]. In our previous work [13], for time-domain control of argon–hydrogen plasma properties in pulse-modulated mode the critical/limiting values of off-times for corresponding on-times have been reported both experimentally and numerically.

In this paper, we present both simulated and experimental determinations reflecting the transient responses of argon and hydrogen-admixed argon plasmas. The effects of SCL and hydrogen concentration upon the spatial distributions of temperature and other plasma parameters were investigated. Time-dependent integrated radiation intensities of atomic argon at 751 nm for different SCL were predicted from the temporal temperature fields and these intensities were used to calculate different response times. Pulse-modulated plasma was generated with argon (100 l/min) and a nonhomogeneous mixture of argon–hydrogen (100/2.5 l/min) as working gas, injecting through the sheath channel of the induction plasma torch. A specially designed torch having eight-turn coil with a large axial length of 144 mm was used to maintain the discharge. Note that the long coil length must improve the materials processing, since a particle will be in plasma-contact for longer time. Spectroscopic measurements of temporal radiation intensities of ArI (751 nm) at different SCL were carried out. Different response times were calculated from the measured temporal intensity distributions. Finally, part of the simulated results was compared with the experimental determinations where acceptable agreements were noticed. The reasons for small deviation of the simulated results from those of experimental ones are discussed elaborately.

Manuscript received February 14, 2001; revised November 19, 2001.

M. M. Hossain, Y. Hashimoto, Y. Tanaka, and T. Sakuta are with the Department of Electrical and Electronic Engineering, Faculty of Engineering, Kanazawa University, Kanazawa 920-8667, Japan (e-mail: 4129hoss@ec.t.kanazawa-u.ac.jp).

K. C. Paul is with the Department of Electrical and Computer Engineering, University of Toronto, Toronto, ON M5S 3G4, Canada.

Publisher Item Identifier S 0093-3813(02)02467-0.

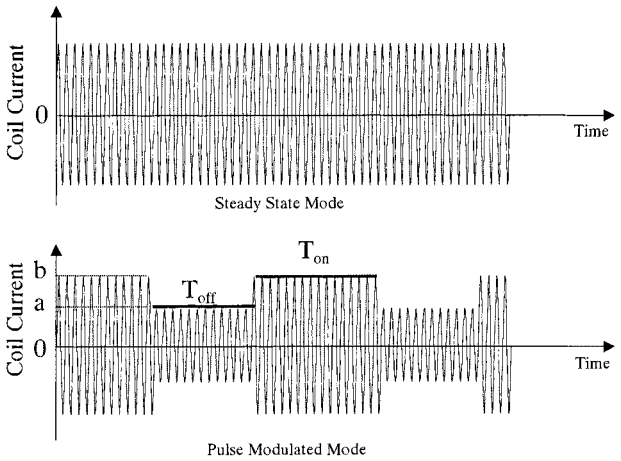

Fig. 1. Concept of pulse-modulated induction thermal plasma.

II. Concept of Pulse Modulation

The concept of pulse modulation of coil current for the generation of induction thermal plasma is described in Fig. 1. Here the radio frequency coil current is amplitude-modulated with a low-frequency (several tens of Hertz) pulsing signal and the modulated current is supplied to the coil, which surrounds the plasma torch. Noting Fig. 1, the SCL and DF are defined the following:

$$SCL(\%) = \frac{\text{Amplitude of current pulse during off-time}(a)}{\text{Amplitude of current pulse during on-time}(b)} \times 100$$

$$DF(\%) = \frac{T_{\text{on}}}{T_{\text{on}} + T_{\text{off}}} \times 100$$

where T_{on} and T_{off} are on and off times of pulsing signal, respectively.

The most attractive and unique features of pulse modulation are:

1) input power to plasma can be controlled by changing only the amplitude of the pulsing signal instead of the high amplitude radio frequency coil current;
2) input power to plasma can be controlled in time domain by controlling the duty factor (changing either on-time or off-time) of pulsing signal;
3) periodic changes of different particle density (electrons, ions, neutral atoms, molecules, etc.) in accord with the pulsing signal;
4) successive application of very high and low electromagnetic fields as well as heat flux introduces nonequilibrium effects, which might be very useful in materials processing.

III. Modeling

The model considers coil current pulsation instead of power to have similarity with the experiment and it is based on our last publication [14]. This model solves the time-dependent conservation equations along with the vector potential form of Maxwell's equations, as listed in the Appendix, using the SIMPLER algorithm of Patankar [15]. The algorithm is based on the control volume scheme for solving the transport equations of incompressible fluids. The reasonable assumptions and boundary conditions are the same as those described in [14].

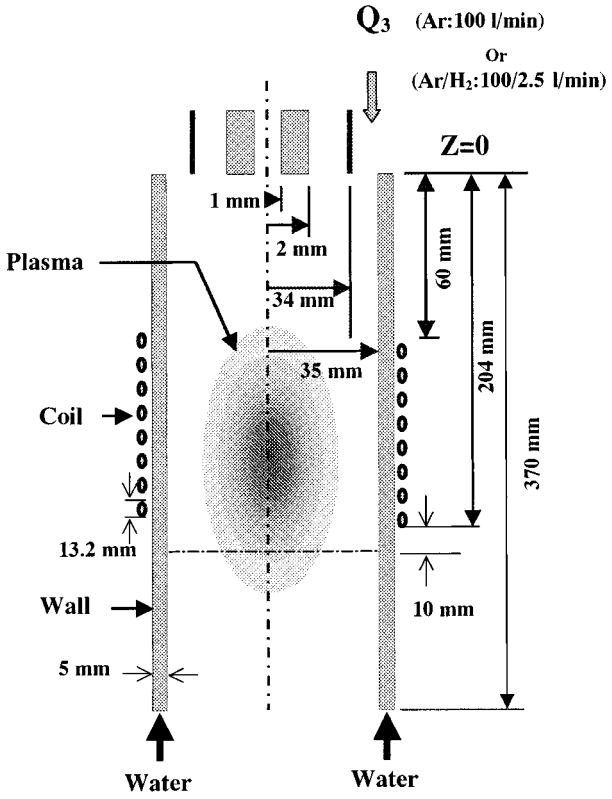

Fig. 2. Schematic diagram of the torch with definitions and dimensions of the parameters, used in simulation.

TABLE I
Operating Conditions

No. of coil turns = 8	Pressure = 760 torr
Frequency = 450 kHz	Pulse on-time = 10 ms
Forward Power = 30/27 kW	Pulse off-time = 5 ms
	Duty factor=67%

Calculation Procedure: Calculation was performed for an RF-ITP torch whose schematics with the definitions of the parameters used in the simulation are described in Fig. 2. Operating conditions are listed in Table I. The time step of each iteration was 10 μ(s) throughout the calculation. The calculations were carried out for a nonuniform grid system having 36 radial and 92 axial nodes.

Thermodynamic Properties: Thermodynamic properties of argon and hydrogen gases required for simulation include viscosity, electrical conductivity, thermal conductivity, mass density, specific heat at constant pressure, and radiative loss coefficient. The first five properties were taken from [16] and the radiative loss coefficient of argon was taken from [17]. The radiative loss coefficient of hydrogen was not available in literature. However, it is anticipated that an estimate must be better than the total neglect. Therefore, the radiative loss coefficient of hydrogen was considered the same as that of argon for any temperature. Nevertheless, a database for radiative loss coefficient of hydrogen was generated based on the work of Tanaka *et al.* [18] and used for a test calculation. Comparing the temperature, calculated using radiative loss coefficient of hydrogen, with that predicted in this work, the maximum difference was

TABLE II
COIL CURRENT FOR AR AND Ar–H_2 PLASMAS AT DIFFERENT SCLS

Ar Plasma		Ar-H_2 Plasma	
SCL(%)	Coil Current [A]	SCL(%)	Coil Current [A]
100	189.3	100	213.9
87	164.9	87	186.3
79	149.9	77	166.0
72	136.5	72	155.0
65	122.7	63	136.0
50	94.6	55	118.5
40	75.7	45	96.7

found at 10%. Thus, we assume that the error caused due to radiative loss coefficient would be less than 10%.

A. Simulated Results

In simulation, we fixed the plasma power at 27 kW before pulsation, considering the 90% overall efficiency of the inverter-feed power supply unit that was used in the experiment with 30-kW forward power. It was found that at a constant power of 27 kW, the coil current was increased by 13% for 2.4% H_2 inclusion. The tabulated coil current for argon and hydrogen-admixed argon plasmas at 27 kW of plasma power for different SCL is presented in Table II. The steady-state coil currents for pure argon and 2.4% hydrogen-admixed argon plasmas were 189.3 and 213.9 A, respectively. The higher specific heat and thermal conductivity of hydrogen versus those of argon and the dissociation of molecular hydrogen were the main reason for such increase of coil current; as in induction plasma, coil current is the only way through which plasma is empowered externally.

The spatial distributions of temperature for a complete cycle of pulsed power are described in Fig. 3(a) and (b) for Ar and Ar–H_2 plasmas, respectively. These figures, which are drawn for 72% SCL, clearly explain the repetitive nature of pulsing plasma. Comparing Fig. 3(a) and (b), it can be noticed that the hottest cores of plasma became larger due to the H_2 inclusion. Moreover, for the inclusion of molecular hydrogen, the high temperature zones except the hottest core shrank over the whole cycle. These effects indicate that plasma has a tendency to concentrate within the mid-coil region, which in turn implies that the reactive zone of plasma shrinks due to the hydrogen inclusion. The dissociative recombination and slow ionization process of a hydrogen atom is mainly responsible for such an effect [19]. For such characteristics, molecular gas is usually used to shrink plasma and thus to protect walls from high temperature. The heat loss reduction results from the temperature decrease by the hydrogen dissociation near the torch wall. As described earlier at the beginning of this section, this is a constant-power plasma of 27 kW and thus hydrogen inclusion has increased the coil current by 13% due to the necessary energy for H_2 dissociation with maintaining energy balance. On the other hand, hydrogen inclusion reduced the heat loss through the torch wall in the mid-coil region, as plasma was constricted in this region due to hydrogen inclusion.

The effects of SCL on the spatial distribution of temperature for Ar and Ar–H_2 plasmas are described in Fig. 4(a) and (b), respectively. These distributions are obtained for an instant while the off-pulse ends. These figures reveal how the hottest core of plasma shrank both axially and radially with the decrease of SCL. The shimmer current level is a measure to specify the effective input power, sufficient to maintain plasma discharge, without extinction for a certain pulse off-time. When the shimmer current level was decreased, the input power to plasma, during off-pulse, decreased, which in turn caused to decrease the plasma temperature. The decrease of temperature at significantly lower SCL was more profound in Ar–H_2 plasma compared with that in Ar plasma (see the figures for 45% SCL). This behavior of Ar–H_2 plasma is explained as follows. Molecular hydrogen needs energy for dissociation. When the SCL is very low (*viz.* 45%), the power loss in hydrogen dissociation (0.15 kW) is pretty significant compared to the total plasma power (1.4 kW), and therefore the overall plasma temperature was found to decrease rigorously.

The effects of hydrogen inclusion upon the radial temperature fields at some distinct axial positions ($z = 58, 130$, and 250 mm) are depicted in Fig. 5(a). In general, plasma temperature is high in the coil region ($z = 60 - 240$ mm) because RF plasma is fed through the coil and hence the electromagnetic fields in this region are very strong. In the coil region, the effect of H_2 inclusion upon the plasma temperature was found to be less significant (see the figure for $z = 130$ mm) compared to the temperature at above ($z = 58$ mm) or below ($z = 250$ mm) the coil. It is also seen from Fig. 5(a) that the H_2 admixing effect is pronounced around the radial position of 22.5 mm $< r < 32$ mm for any axial position of plasma. Thus, the H_2 admixing effect is found to be profound around the highly dissociation/ionization range of temperature (4000–8000 K) for the reason explained above. The axial temperature profiles describing the H_2 admixing effects upon argon plasma, at three different radial positions ($r = 0, 17.5$, and 30.5 mm), are presented in Fig. 5(b). The effects of H_2 inclusion upon the plasma temperature drop were very significant near the wall ($r = 30.5$ mm) along the torch length; here, H_2 dissociation played the major role. Hydrogen inclusion effect upon the plasma temperature was almost alike on the axis of symmetry ($r = 0$) and at the middle from axis of symmetry and wall (viz. $r = 17.5$ mm); plasma temperature decreased both above and below the coil region, where both dissociation and ionization had the impact on such behavior.

The variation of axial velocity of flow with time at two specific locations along the centerline of the discharge has been presented in Fig. 6. It is observed from the figure that the variation of velocity is stronger at 10 mm below the coil end ($z = 214$ mm) than that of at midcoil region ($z = 132$ mm). The addition of H_2 reduced the relaxation time of axial velocity at $z = 214$ mm, during both on and off-pulsing transition.

The time-dependent integrated radiation intensity of atomic argon spectral line (751 nm) for Ar and Ar–H_2 plasmas was predicted from the temporal temperature distributions using the following equations:

$$I_z = 2\pi \int_0^{R_0} I(T, r) r dr \tag{1}$$

and

$$I(T, r) = \frac{1}{4\pi} \frac{hcgAN(T)}{\lambda Z(T)} e^{\frac{-E_n}{kT}} \tag{2}$$

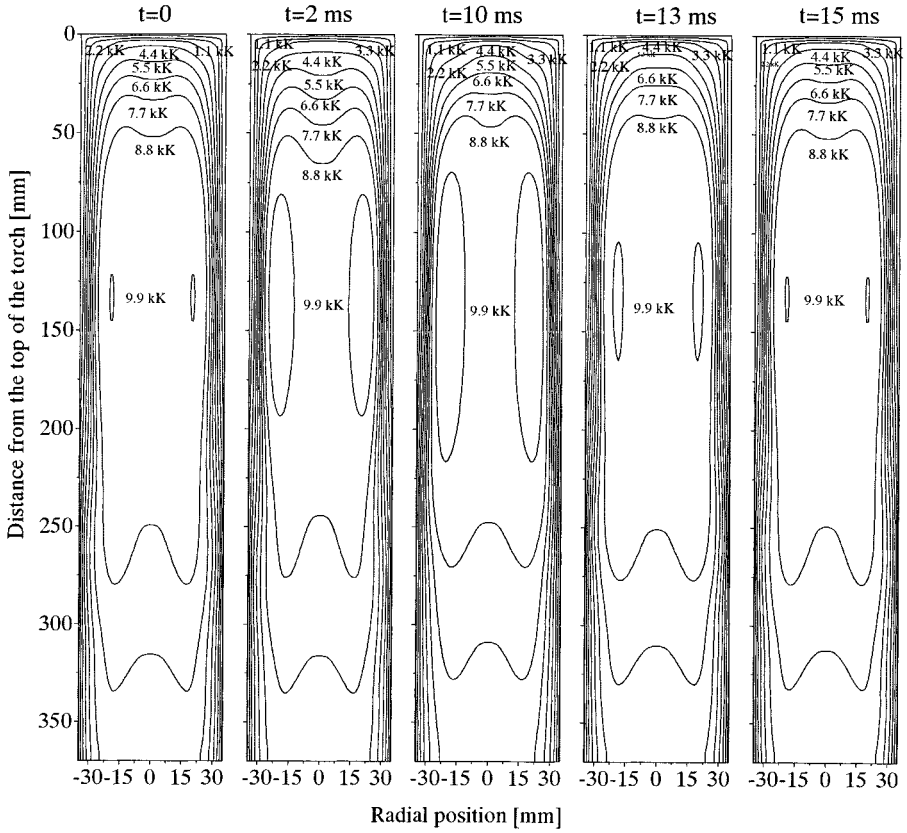

(a)

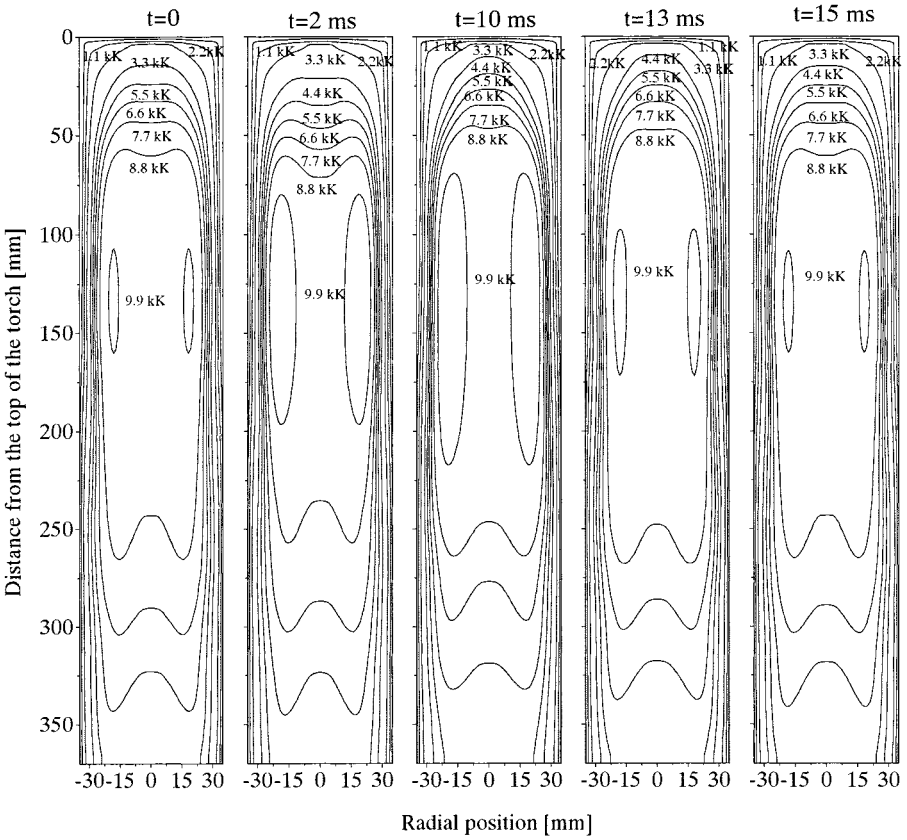

(b)

Fig. 3. Spatial distribution of temperature at 72% SCL for (a) Ar and (b) Ar–H_2 plasmas, at distinct time instants over a cycle of pulsing signal.

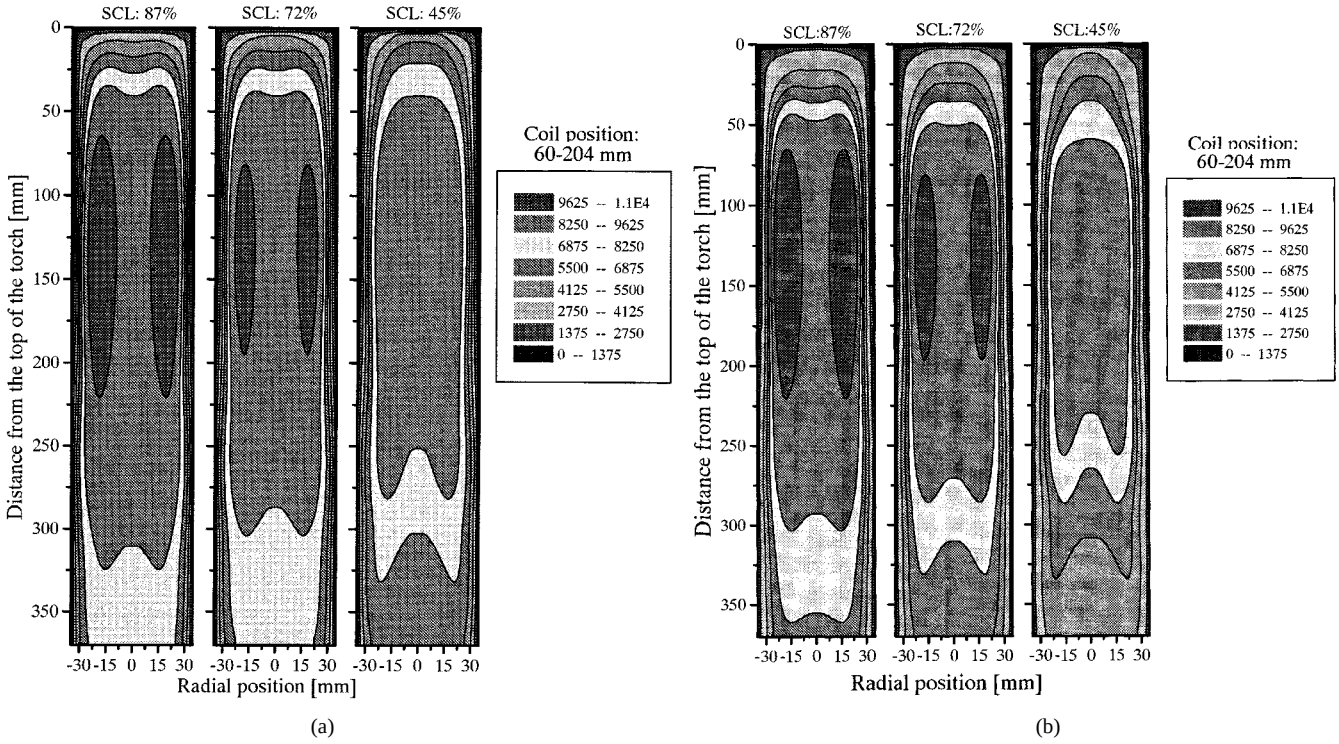

Fig. 4. SCL effect upon the spatial temperature distributions of Ar (a) and Ar–H_2 (b) plasmas predicted at the end of off-pulse.

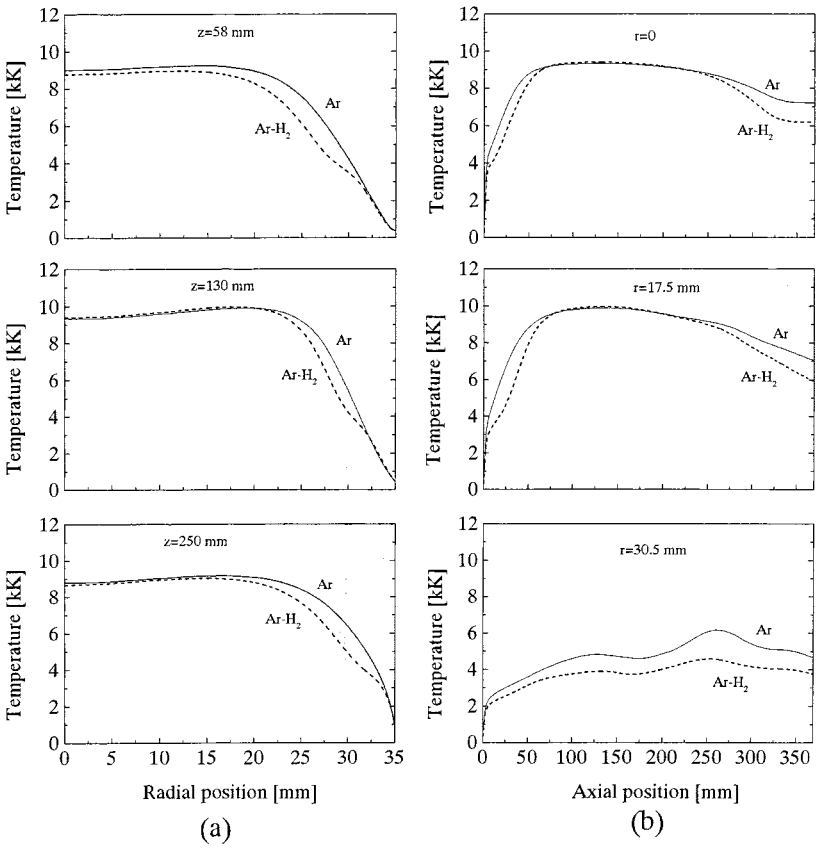

Fig. 5. Hydrogen admixing effects upon the (a) radial and (b) axial temperature distributions of Ar plasma.

where I_z is the integrated radiation intensity at a particular axial position, h is Planks constant, c and λ are velocity and wavelength of light, respectively, g is the statistical weight, A is the transition probability for spontaneous emission, $N(T)$ and $Z(T)$ are temperature-dependent particle density and internal partition function, respectively, E_n is the upper energy level, k is the Boltzmann's constant, and T is the temperature.

Fig. 7(a) and (b) represents the SCL effects upon the time-dependent integrated radiation intensity of ArI for Ar and Ar–H_2 plasmas, respectively. These results were obtained at an axial

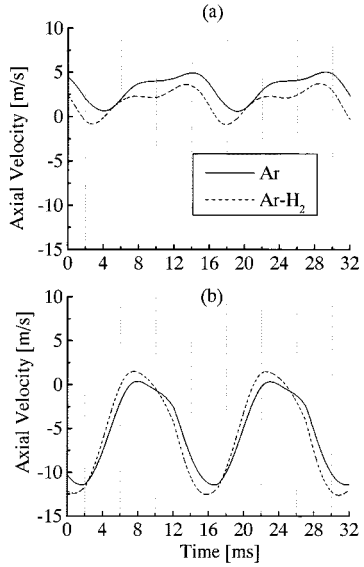

Fig. 6. The variation with time of the axial velocity of the flow at (a) mid-coil region and (b) 10 mm below the coil end along the center line of the discharge $(r = 0)$.

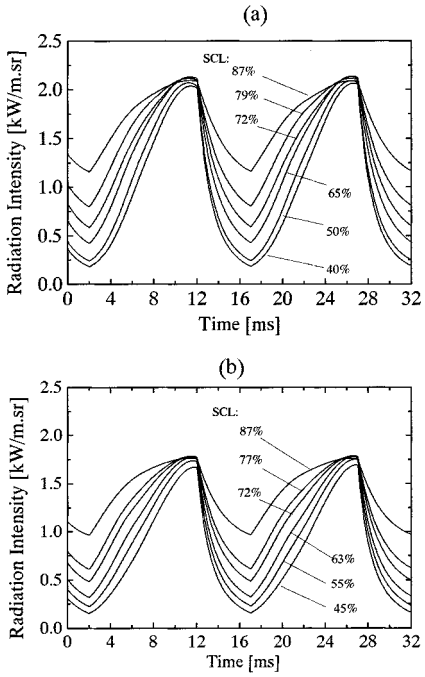

Fig. 7. SCL effect upon time-dependent integrated radiation intensities of ArI (751 nm) for (a) Ar and (b) Ar–H_2 plasmas, predicted at 10 mm below the end coil.

position of 214 mm (10 mm below the coil end). The collisional excitation process between electron and heavy particles takes very little time (about 10^{-7}s) and the de-excitation process through photon emission was extremely fast as the lifetime of excited state was very short (less than 10^{-9}s) [20]. Thus, the relaxation time of the spectroscopic radiation process was negligible. Hence, the temporal change of integrated radiation intensity corresponded to that of plasma itself. It can be seen from the figures that the hydrogen inclusion in the argon plasma dropped the integrated intensity range because the temperature happened to decrease at some radial points due to H_2 inclusion. The maxima of the intensities corresponding to SCLs were

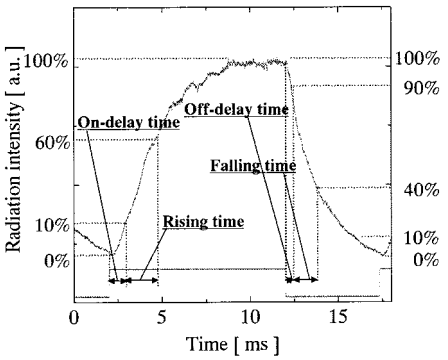

Fig. 8. Definitions of different response times of plasma.

found almost similar in both plasmas, although the minima were fully discrete. The reason is that the coil current, which feeds the plasma, was the same during on-time for any SCL but it was different during off-time for different SCLs, due to which the plasma energy and thus the temperature was different. At lower SCL, plasma power and thus temperature was lower; therefore, the integrated intensity dropped to lower level.

Different response times or characteristics times such as on-delay, rising, off-delay, and falling time were calculated from the temporal radiation intensity illustrated in Fig. 7. The response/characteristics times are schematically shown in Fig. 8. The on-delay time is the time required to raise the intensity from base level to 10%, after triggered-on by the pulsing signal; similarly, off-delay time is the time required for the intensity to drop to 90% from maximum level just after triggered-off of the pulsing signal. The rising and falling times are the times needed for the intensity to raise from 10% to 60 and to drop from 90% to 40%, respectively. During the on-pulse, the collision between electron and heavy particles is the dominating mechanism of energy exchange. Thus, the rising time reflects the effectiveness of the collisional process. On the other hand, during off-pulse, the collision as well as slow conduction and convection processes cause the energy transfer. So, falling time is a measure of the effectiveness of these processes. On-delay and off-delay times are the measures of ease of state change during off-to-on pulse and on-to-off pulse transition, respectively. In other words, on-delay and off-delay times depend on the depth of the power level. The calculated response times can be seen in later figures (Figs. 13 and 14) because these times were compared with the experimentally obtained response times there in Section V. Regardless, the theoretical predictions did not reveal any significant effect upon the on-delay and off-delay times for the inclusion of hydrogen in argon plasma. The on-delay time was found to decrease slightly with the increase of SCL, whereas the off-delay time remained almost unchanged with SCL. From the rising time profile it was found that the plasma response became a bit slower due to the inclusion of hydrogen at lower SCL. However, SCL or hydrogen admixing did not affect the falling time.

IV. Experimental Approach

A. Experimental Setup

Fig. 2 describes the schematic geometry and dimensions of the induction plasma torch. The torch has a standard config-

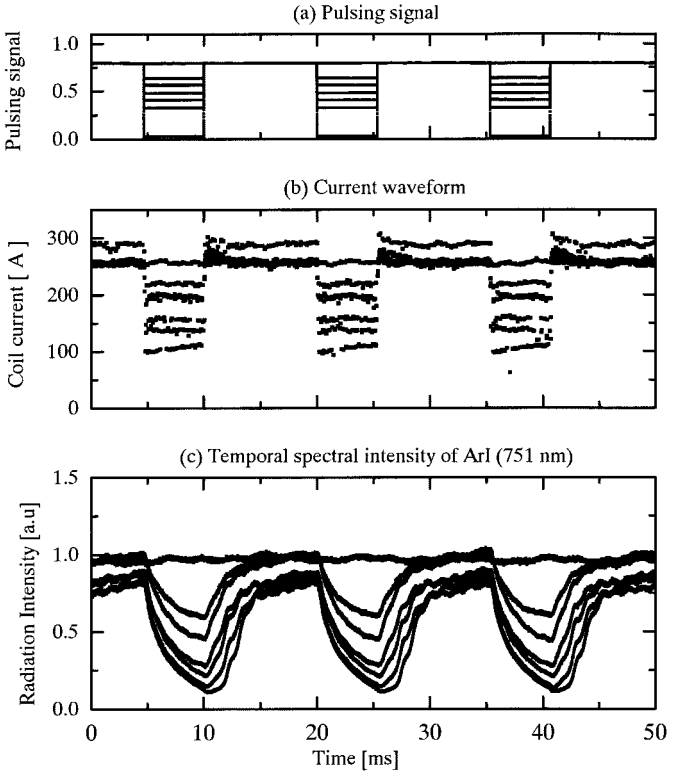

Fig. 9. (a) Spectroscopically measured temporal pulsing signal, (b) modulated current waveform peaks, and (c) radiation intensity of atomic argon at 10 mm below the coil-end for Ar plasma.

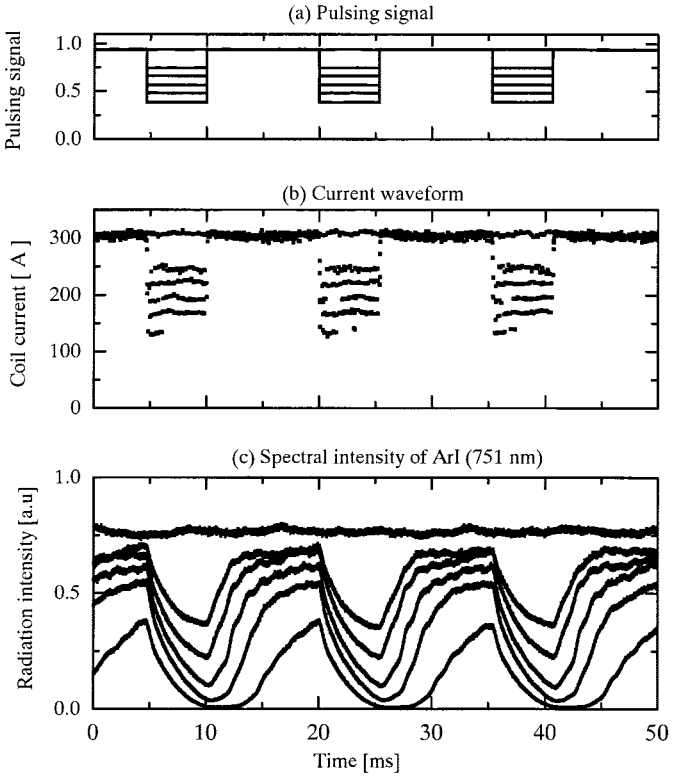

Fig. 10. (a) Spectroscopically measured temporal pulsing signal, (b) modulated current waveform peaks, and (c) radiation intensity of atomic argon at 10 mm below the end coil for Ar–H_2 plasma.

uration of two co-axial tubes of 370-mm length surrounded by a water-cooled RF-coil. The inner diameter of the inner quartz tube and the outer diameter of the outer Pyrex tube are 70 and 95 mm, respectively. In order to protect the torch from overheating, cooling water was passed through in the upward direction between the quartz and Pyrex tubes. The torch has three inlets, namely carrier, plasma, and sheath channel, for gas injection, although the gas was injected through the sheath channel with a 30° swirl from the outer slots of the gas distributor. A solid state amplifier (HF0030W45MS, Fuji Electric Co., Ltd.) was employed for the power supply. The MOSFET-employed inverter-feed power source continuously supplied the electric power of 50 kW (maximum) with a nominal frequency of 450 kHz and has a high matching efficiency of about 90%. The RF current was amplitude-modulated by a low-frequency (67 Hz) pulsing signal to achieve current pulsation. The modulated current signal was then supplied to the RF-coils through a series LC resonance circuit, which was used for impedance-matching purposes. An optical system with a spatial resolution of 1 mm was employed to obtain the plasma emission. Atomic argon line intensity at 751 nm was measured using a monochromator (JOBIN YVON HR-320) and detected by a photomultiplier (Hamamatsu R1104) of 70 ns response time. The detected signal was digitized and stored by a multichannel digitizer (DL706E, Yokogawa Electric Co.) with minimum sampling time of 0.5 μ(s) per address.

B. Spectroscopic Measurements

Spectroscopically measured temporal radiation intensities of ArI (751 nm) along with the pulsing signal and coil current for Ar and Ar–H_2 plasmas are presented in Figs. 9 and 10, respectively. The point of measurement was 10 mm below the downstream coil ($z = 214$ mm). The operating conditions are the same as those used in simulations (Table I). It can be seen from Figs. 9(b) and 10(b) that the magnitude of coil current was increased by the inclusion of hydrogen into argon plasma. The plasma density drops due to addition of hydrogen in the argon plasma. Eventually, the dissociative recombination reactions [21] are responsible for the loss of charged particles like electron. The details of the reaction rates are beyond the scope of this article. The reaction rates discussed by Tanaka and Sakuta [22] for transient SF_6 plasma show that the time constants for various species are within microsecond order. The range of these time constants is far below the order seen in plasma fluctuation, where time constants are in the range of millisecond order. Therefore, the dissociation and recombination rates would slightly affect the findings for time constants. In induction plasma, electrons from the induced electromagnetic field primarily absorb the electrical energy transferred to the plasma and thus the only way for energy input to plasma is through the coil current. The thermal conductivity of hydrogenated-argon plasma must be higher compared with that of argon plasma because hydrogen has higher thermal conductivity. Therefore, the coil current has to rise in order to compensate the enhanced thermal conduction loss as well as the loss of electron due to dissociative recombination of hydrogen. Figs. 9(c) and 10(c) show the SCL effects upon temporal radiation intensities of Ar and Ar–H_2 plasmas, respectively. It can be realized from the figures that on-delay and rising times were increased with the lowering of SCL in both plasmas but this

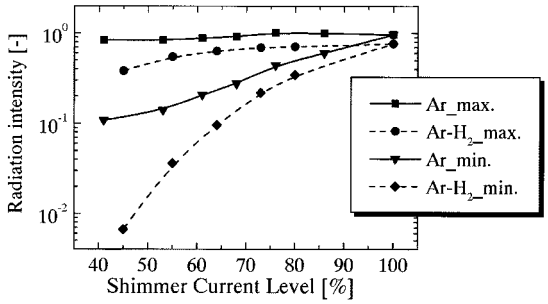

Fig. 11. Hydrogen admixing and SCL effects upon the minimum and maximum levels of radiation intensities, measured at 10 mm below the end coil.

increase was strong in Ar–H_2 plasmas. SCL, however, did not have any effect upon the other response times. Hydrogen inclusion into argon plasma [comparing Figs. 9(c) and 10(c)] slowed down plasma response and this effect was found severe at lower SCL. In general, the intensity was decreased by the inclusion of H_2, as shown in Fig. 11. The minimum levels of intensity for the hydrogenated-argon plasma decreased very profoundly with the lowering of SCL compared with those in argon plasma, whereas , H_2-inclusion did not have any significant effect on the maximum levels for the decrease of SCL.

V. Comparison of Experimental and Simulated Results

For the better comprehension and justification of the deviation between simulated and experimental results, parts of the simulated results are compared in this section with those of experimental determinations.

Experimentally measured radiation intensity of ArI (751 nm) for both Ar [Fig. 12(a)] and Ar–H_2 [Fig. 12(b)] plasmas are compared with those of numerical predictions. The operating conditions for both experiment and simulation were the same as described in Table I. Both in experimental and numerical predictions, the magnitude of intensities changed almost at the same order with the current pulse. For Ar–H_2 plasma, the ratio of maximum to minimum levels of intensity was 3.1 in experiment and 3.7 in theory, though the response was faster in experiment. And those ratios for Ar plasma in experiment and theory were 4.0 and 5.7, respectively.

Response times of plasma were also calculated from the spectroscopically measured intensity for both Ar and Ar–H_2 plasmas following the definitions elucidated in Fig. 8.

The broken lines of Fig. 13 show the experimentally determined SCL effects upon the response times: on-delay, rising and off-delay and falling time, for Ar plasma. The broken lines in Fig. 14 present the same effects for Ar–H_2 plasma. The experimental findings show that on-delay time became longer at lower SCL in both Ar and Ar–H_2 plasmas; this time was extremely long in Ar–H_2 plasma, at 40%. High thermal conductivity and heat capacity of molecular hydrogen gas in Ar–H_2 ITP strongly cooled down the plasma at significantly lower SCL (at or below 55%) during off-pulse, hence it needed longer time to heat up the hydrogen- admixed plasma. As was seen in theory, the rising time decreased gradually with the increase of SCL in the experiment too, but the falling time was almost unchanged in both Ar and Ar–H_2 plasmas. From comparison between theory and experiment it was found that rising time during on-pulsation was, in general, higher in theoretical predictions than that found in experimental measurements. The stronger nonequilibrium conditions of practical plasma just before on-pulsation and near-equilibrium condition just before off-pulsation were responsible for such characteristics of response times. The comparative study of this section can be summarized in the following points.

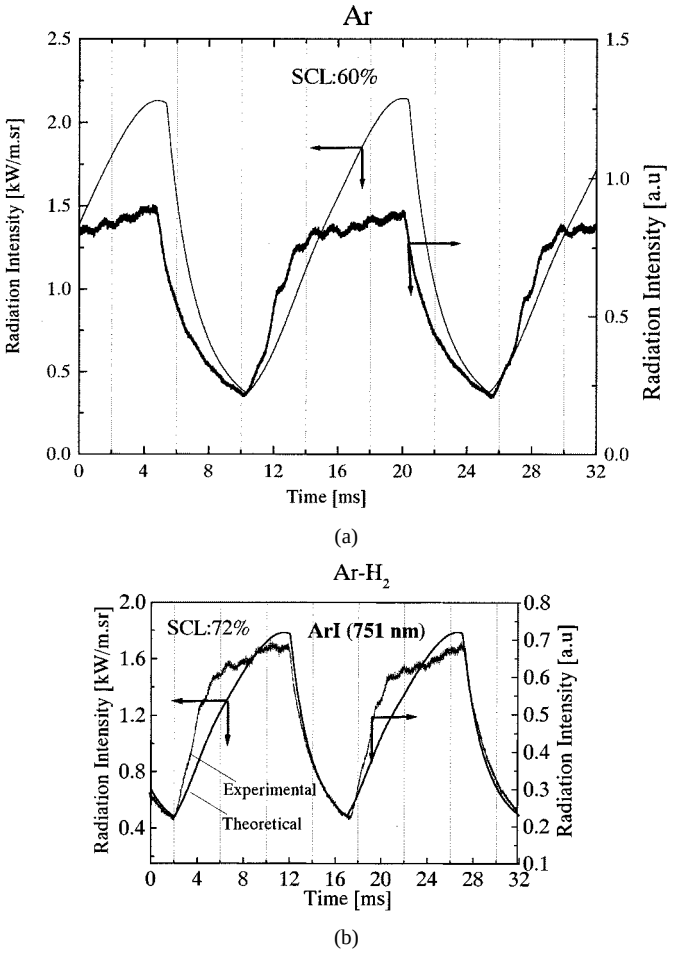

Fig. 12. Comparison of experimental and simulated radiation intensities of ArI (751 nm), for (a) Ar and (b) Ar–H_2 plasmas, measured/predicted at 10 mm below the coil-end ($z = 214$ mm).

1) At the end of off-pulse, practical plasma stays in nonequilibrium condition because the cooler region of plasma is very likely to be in a nonequilibrium condition. Around the end of off-pulse, the plasma temperature becomes low for the following reasons: a) during off-pulse power input is at minimum level and hence temperature drops and b) the continued injection of cold gas through the sheath channel at insignificant power input enhances the cooling action of plasma.
2) At the beginning of on-pulse, due to the sudden application of on-pulse, electrons are accelerated by the high-input energy and thus plasma deviates from equilibrium condition. This nonequilibrium situation dies out with time when energy balance between electrons and heavy particles is reached.
3) Our numerical model considers equilibrium (LTE) condition. Therefore, the numerical predictions have been

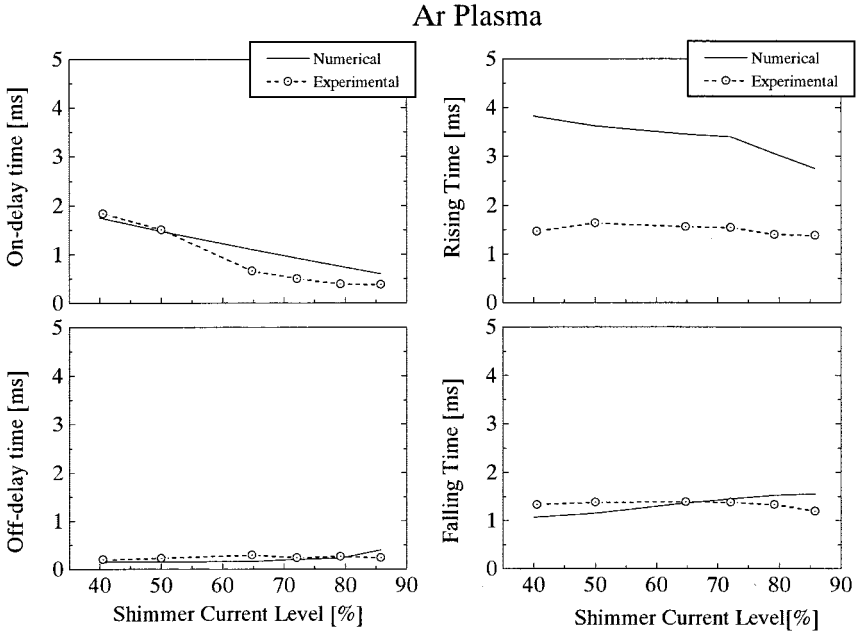

Fig. 13. Comparison of experimental and simulated response times of Ar plasma measured/predicted at 10 mm below the coil-end ($z = 214$ mm).

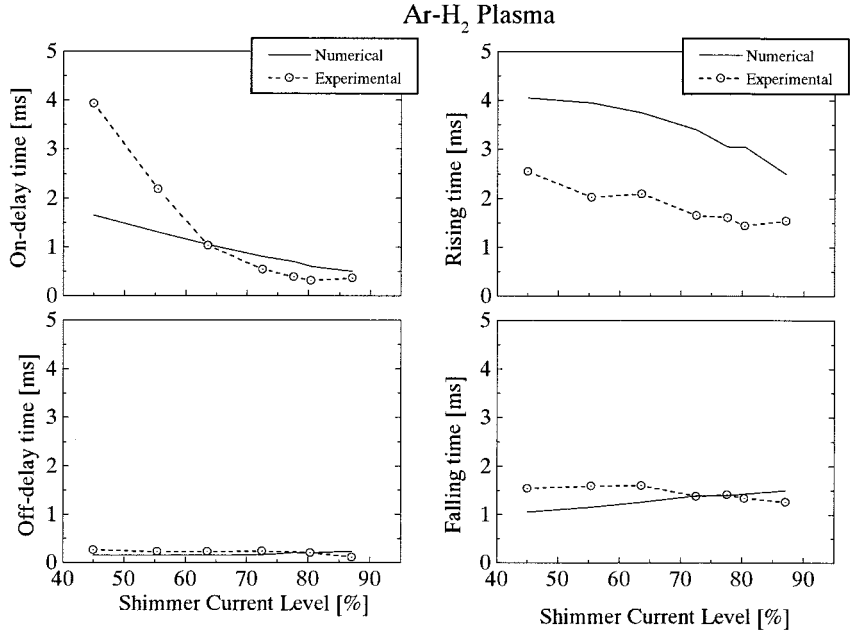

Fig. 14. Comparison of experimental and simulated response times of Ar–H_2 plasma measured/predicted at 10 mm below the coil-end ($z = 214$ mm).

found to differ with the experimental findings due to the above two effects.

4) The discrepancy between theoretical and experimental results has been lowered with the inclusion of H_2 gas in argon plasma because stronger nonequilibrium phenomena of argon plasma moves toward weaker nonequilibrium phenomena by the high thermal conductivity, heat capacity, and the dissociative recombination [20] of hydrogen in the H_2-admixed argon plasma.

VI. Conclusion

Experiments were carried out with a plasma reactor having huge coil length (144 mm) and MOSFET-employed inverter-feed power source. It was possible to control plasma power as well as heat flux by changing SCL from 100% to 40%. For the same operating conditions, a two-dimensional time-dependent LTE model was solved to predict temporal behavior of plasma fields and thus to compare with the experimental results. It was found both in theory and experiment that hydrogen inclusion (2.4%) in argon plasma:

1) slowed down plasma response at lower SCL, especially during on-pulsing transition;
2) caused a decrease in plasma temperature;
3) shrank plasma axially;
4) drove stronger non-LTE plasma toward weaker non-LTE.

Practical pulse-modulated plasma deviated from the LTE condition, even at atmospheric pressure, especially at the vicinity of off- to on-pulsing transition, and attained an almost

LTE condition at the end of on-pulse. At the beginning of on-pulse, plasma response slowed down at lower SCL, but it was not affected by SCL during off-pulse. The discrepancies between experimental and numerical results point out that practical pulse-modulated plasma is very likely to deviate from LTE, especially around the end of off-pulse and the beginning of on-pulse, which our LTE model does not hold. At this stage, our goal is to establish that the pulse-modulated plasma stays out of LTE conditions, even at high pressure, and the inclusion of molecular gas like H_2 drives the plasma toward LTE.

APPENDIX
GOVERNING TIME-DEPENDENT EQUATIONS

The time-dependent conservation equations and vector potential form of Maxwell's equations are as follows.

Mass conservation:

$$\frac{\partial \rho}{\partial t}+\frac{\partial(\rho u)}{\partial z}+\frac{1}{r}\frac{\partial(r\rho v)}{\partial r}=0. \tag{A1}$$

Momentum conservation:

Axial momentum

$$\rho\frac{\partial u}{\partial t}+\rho u\frac{\partial u}{\partial z}+\rho v\frac{\partial u}{\partial r}=-\frac{\partial p}{\partial z}+2\frac{\partial}{\partial z}\left(\mu\frac{\partial u}{\partial z}\right)+\frac{1}{r}\frac{\partial}{\partial r}\left[r\mu\left(\frac{\partial u}{\partial r}+\frac{\partial v}{\partial z}\right)\right]+F_z. \tag{A2}$$

Radial momentum

$$\rho\frac{\partial v}{\partial t}+\rho u\frac{\partial v}{\partial z}+\rho v\frac{\partial v}{\partial r}=-\frac{\partial p}{\partial r}+\frac{\partial}{\partial z}\left[\mu\left(\frac{\partial v}{\partial z}+\frac{\partial u}{\partial r}\right)\right]+\frac{2}{r}\frac{\partial}{\partial r}\left[r\mu\left(\frac{\partial v}{\partial r}\right)\right]+F_r. \tag{A3}$$

Energy conservation

$$\rho\frac{\partial h}{\partial t}+\rho u\frac{\partial h}{\partial z}+\rho v\frac{\partial h}{\partial r}=\frac{\partial}{\partial z}\left(\frac{\lambda}{C_p}\frac{\partial h}{\partial z}\right)+\frac{1}{r}\frac{\partial}{\partial r}\left(r\frac{\lambda}{C_p}\frac{\partial h}{\partial r}\right)+P^o-R^o. \tag{A4}$$

Vector potential form of Maxwell's equations:

$$\frac{\partial^2 A_\theta}{\partial z^2}+\frac{1}{r}\frac{\partial}{\partial r}\left(r\frac{\partial A_\theta}{\partial r}\right)-\frac{A_\theta}{r^2}=j\mu_0\sigma\omega\boldsymbol{A}_\theta \tag{A5}$$

where t is time; ρ is mass density; μ is viscosity; λ is thermal conductivity; h is enthalpy; p is pressure; C_p is specific heat at constant pressure; F_z and F_r are axial and radial Lorentz forces, respectively; u and v are axial and radial velocities; P° is volumetric Joule heating; R° is volumetric radiative loss; $\boldsymbol{A}_\theta$ is phasor of vector potential; $\omega=2\pi f$ (f is the frequency of coil current); μ_0 is permeability of vacuum; and j is the complex vector.

REFERENCES

[1] A. E. Mensing and L. R. Boedeker, "Theoretical investigation of r.f. induction heated plasmas," NASA , CR-1312 , 1969.

[2] J. Mostaghimi and M. I. Boulos, "Two-dimensional electromagnetic field effects in induction plasma modeling," *Plasma Chem. Plasma Process*, vol. 9, pp. 25–44, 1988.

[3] X. Chen, "Heat transfer and flow in a radio frequency plasma torch—A new approach," *Int. J. Heat Mass Transfer*, vol. 33, pp. 815–826, 1990.

[4] J. Mostaghimi, P. Proulx, and M. Boulos, "A two-temperature model of the inductively coupled R.F. plasma," *J. Appl. Phys.*, vol. 61, pp. 1753–1760, 1987.

[5] S. H. Paik and E. Pfender, "Modeling of an inductively coupled plasma at reduced pressures," *Plasma Chem. Plasma Process*, vol. 10, pp. 167–188, 1990.

[6] J. Mostaghimi and M. Boulos, "Effect of frequency on local thermodynamic equilibrium conditions in an induction coupled argon plasma at atmospheric pressure," *J. Appl. Phys.*, vol. 68, pp. 2643–2648, 1990.

[7] P. Meubus, "Transient conditions in inductively heated plasmas: Thermodynamic equilibrium and temperature measurements," *Can. J. Phys.*, vol. 60, pp. 886–892, 1982.

[8] J. M. de Regt, V. der Mullen, and D. C. Schram, "Responses of the electron density and temperature to the power interruption measured by Thompson scattering in an inductively coupled plasma," *Phys. Rev.*, vol. 52, pp. 2982–2987, 1995.

[9] F. H. A. Fey, W. W. Stoffels, J. A. M. van der Mullen, B. van der Sijde, and D. C. Schram, "Instantaneous and delayed responses of line intensities to interruption of the RF power in an argon inductively coupled plasma," *Spectrochim. Acta*, vol. 46B, pp. 885–900, 1991.

[10] T. Suekane, T. Taya, Y. Okuno, and S. Kabashia, "Numerical studies on the nonequilibrium inductively coupled plasma with metal vapor ionization," *IEEE Trans. Plasma Sci.*, vol. 24, pp. 1147–1154, 1996.

[11] J. Mostaghimi, K. C. Paul, and T. Sakuta, "Transient responses of the radio frequency inductively coupled plasma to a sudden change in power," *J. Appl. Phys.*, vol. 83, pp. 1898–1908, 1998.

[12] T. Sakuta, K. C. Paul, M. Katsuki, and T. Ishigaki, "Experimentally diagnosed transient behavior of pulse modulated inductively coupled thermal plasma," *J. Appl. Phys.*, vol. 85, pp. 1372–1377, 1999.

[13] M. M. Hossain, K. C. Paul, Y. Tanaka, T. Sakuta, and T. Ishighaki, "Prediction of operating region of pulse-modulated radio frequency inductively coupled thermal plasma," *J. Phys. D: Appl. Phys.*, vol. 33, pp. 1843–1853, 2000.

[14] K. C. Paul, M. M. Hossain, Y. Hashimoto, Y. Tanaka, and T. Sakuta, "Responses of a long-coil pulse modulated induction plasma," *IEEE Trans. Plasma Sci.*, vol. 29, pp. 326–334, Apr. 2001.

[15] S. V. Patankar, *Numerical Fluid Flow and Heat Transfer*. New York: Hemisphere, 1980.

[16] M. I. Boulos, P. Fauchais, and E. Pfender, *Thermal Plasmas—Fundamentals and Applications*. New York: Plenum, 1994, vol. 1.

[17] D. L. Evans and R. S. Tankin, "Measurement of emission and absorption of radiation by an argon plasma," *Phys. Fluids*, vol. 10, pp. 1137–1144, 1967.

[18] Y. Tanaka, K. C. Paul, and T. Sakuta, "Thermodynamic and transport properties of N_2/O_2 mixtures at different admixture ratios," *Trans. IEE Japan*, vol. 120-B, no. 1, pp. 24–30, Jan. 2000.

[19] M. Andrieux, J. M. Badie, M. Ducarroir, and C. Bisch, "The evolution of the translationalenergy of hydrogen atoms in a 2 MHz inductively coupled plasma deposition reactor," *J. Phys. D: Appl. Phys.*, vol. 31, pp. 1457–1464, 1998.

[20] W. L. Wiese, M. W. Smith, and B. M. Glennon, *Atomic Transition Probabilities*. Washington DC: NSRDS-NBS, 1969, vol. II.

[21] R. P. Dahiya, K. Hari, M. C. M. van de Sanden, and D. C. Schram, "Molecular processes in Ar–H_2 expanding thermal plasma," in *Proc. 13th Int. Symp. Plasma Chem.*, Beijing, China, Aug. 1997, pp. 541–45.

[22] Y. Tanaka and T. Sakuta, "Numerical approach for analysing transient behavior of SF6 induction thermal plasma using reaction kinetics," in *Proc. 14th Int. Symp. Plasma Chem.*, Prague, Czech Republic, Aug. 1999, pp. 245–250.

M. M. Hossain (S'99) was born on December 1, 1969. He received the B.S. degree from Bangladesh University of Engineering and Technology, Dhaka, Bangladesh, in 1994, and the M.S. degree from Kanazawa University, Japan, in March 2000, in electrical and electronic engineering. He is currently pursuing the Ph.D. degree at the same university.

Since April 1994, he has been working as a Lecturer in the Department of Electrical and Electronic Engineering, Bangladesh Institute of Technology, Chittagong, Bangladesh. Recently, he became an Assistant Professor of the same department. His research interests include radio frequency induction thermal plasma for plasma processing.

Y. Hashimoto was born in 1975. He received the B.S. and M.S. degrees in electrical and electronic engineering from Kanazawa University, Japan, in 1998 and 2000, respectively.

Presently he is working at NTT, Japan. His research interests include radio frequency inductively coupled plasma.

Y. Tanaka was born in Japan on November 19, 1970. He received the B.S., M.S., and Ph.D. degrees in electrical engineering from Nogoya University, Japan, in 1993, 1995, and 1998, respectively.

He has been working as a Research Associate in the Department of Electrical and Electronic Engineering, Kanazawa University, Japan, since April 1998. His research interests include the arc interruption phenomena and thermal plasma applications.

K. C. Paul (M'99) was born on July 1, 1965. He received the B.S. degree in 1990 from the Department of Electrical and Electronic Engineering, Bangladesh Institute of Technology, Chittagong, Bangladesh, and the M.Eng. and D.Eng. degrees in 1995 and 1998, respectively, from Kanazawa University, Japan.

He was a Japan Society for the Promotion of Science post-doctoral research fellow at Kanazawa University, Japan, from April 1998 to March 2000. Presently, he is working in the Electrical and Computer Engineering Department of Toronto University, Canada, as a Research Fellow. His research interests include RF-ICPs, circuit breakers, and dc lamp arcs.

Tadahiro Sakuta (M'91) was born on January 3, 1950. He received the Ph.D. degree in electrical engineering from the Department of Electrical Engineering, Nagoa University, Japan, in 1980.

In April 1981, he was appointed a Research Associate in the same Department. Since April 1988, he has been working as an Associate Professor and then as a Professor in the Department of Electrical and Electronic Engineering, Kanazawa University, Japan. His research interests include the diagnosis and application of high-pressure thermal plasma including inductively coupled plasma and circuit breaker arcs.

Dr. Sakuta is a Member of the Society of Applied Physics and Institute of Electrical Engineers (IEE) of Japan.